MODELING OF CRYOGENIC HYDROGEN JETS

Giannissi, S.G.[1,2], Venetsanos, A.G.[1], Markatos, N.[2]
[1]Environmental Research Laboratory, National Centre for Scientific Research Demokritos, Aghia Paraskevi, Athens, 15310, Greece, sgiannissi@ipta.demokritos.gr, venets@ipta.demokritos.gr
[2]School of Chemical Engineering, National Technical University of Athens, Heroon Polytechniou 9, 15780, Athens, Greece, n.markatos@ntua.gr

ABSTRACT

In the present work the CFD modeling of cryogenic hydrogen releases in quiescent environment is presented. Two tests from the series of experiments performed in the ICESAFE facility at KIT (Karlsruhe Institute for Technology) have been simulated within the SUSANA project. During these tests hydrogen at temperature of 37K and 36K and at pressure of 19 and 29 bars, respectively, is released horizontally. The release at the nozzle is sonic and the modeling of the under-expanded jet was performed using two different approaches: the Ewan and Moodie approach and a modification of the Ewan and Moodie approach (modified Ewan and Moodie) that is introduced here and employs the momentum balance to calculate the velocity in the under-expanded jet. Using these approaches a pseudo-diameter is calculated and this diameter is set as source boundary in the simulation. Predictions are consistent with measurements for both experiments with both approaches. However, the Ewan and Moodie approach seems to perform better.

1.0 INTRODUCTION

One of the issues that hydrogen energy community has to deal with is the transportation and storage of hydrogen in an efficient way. One method is to liquefy hydrogen and to transport and store it at low temperatures and high pressures. However, the flammable nature of hydrogen raises safety concerns. Little information was available for safety analysis regarding release of liquid pressurized hydrogen through small breaks until recently. In 2012 a series of experiments [1] was performed by KIT (Karlsruhe Institute for Technology), in order to investigate the behavior of cryogenic jets through a small break. Hydrogen distribution experiments and ignition experiments were performed. For the un-ignited jets a correlation was proposed for predicting the axial hydrogen concentration dependent on the nozzle diameters and the cryogenic reservoir conditions. The proposed correlation can describe satisfactory the axial hydrogen distribution close to the release before the jet buoyancy region. The correlation was a least square data fit from the measurements with different reservoir conditions and nozzle diameters. The measurements showed a linear tendency when they were plotted against a density-scaled distance.

In order to predict the jet behavior over the whole domain CFD modeling can be employed. CFD simulations have been proved a reasonably trustworthy and useful tool in predicting physical phenomena, such as jet releases. Previous works [2,3] had shown the good predicting capabilities of CFD tools for gas releases. In [4] simulation of pressurized hydrogen release was carried out and the results were in good agreement with the measurements.

In the present study, carried out in the framework of the SUSANA project [5] the CFD performance in predicting cryogenic jet releases is examined. For the simulations, the ADREA-HF CFD code is used and the modeling strategy is based on the guide to best practices in numerical simulations [6] that is developing within the SUSANA project.

Two tests from the KIT un-ignited jet experiments are simulated, IF 3000 and IF 3004 with mass flow rates 0.00455 and 0.00802 kg/sec, respectively. The reservoir pressure and temperature conditions are 19 bars, 37 K and 29 bars, 36 K for the IF 3000 and the IF 3004, respectively.

Two approaches were used to model the under-expanded jet: the Ewan and Moodie [7] and a modification of the Ewan and Moodie approach (modified Ewan and Moodie) which is introduced here and employs the momentum balance similar to the Birch 87 approach [8], in order to calculate the velocity at the notional nozzle.

The predicted hydrogen concentration at steady state along the jet centerline is compared with the measured concentration. Predictions of both experiments are consistent with the measurements using both approaches. However, the Ewan and Moodie approach exhibited better performance in both experiments.

2.0 EXPERIMENTAL DESCRIPTION

The experiments were performed inside a test chamber of hydrogen test site HYKA at KIT. The dimensions of the chamber were 8 x 5.5 x 3.4 m. The chamber was large enough compared to the jet region and it may be considered that it does affect the jet. Detailed description of the facility, the instrumentation and the operation of cryogenic jet release experiments may be found in [1].

The hydrogen was released horizontally in quiescent atmosphere and the release was sonic. Prior to the release the hydrogen was cooled down to low temperatures ranged from 34-65 K and it was compressed under high pressures varied from 7-30 bars. A series of 26 experiments were performed to investigate the hydrogen distribution, while a series of 11 experiments were performed to investigate the hydrogen combustion.

For the hydrogen distribution investigation a nozzle of 1 mm and 0.5 mm diameter was used in the test series IF 3000 and in the test series IF 5000, respectively. In the present study the tests IF 3000 and IF 3004 from the series IF 3000 were considered for simulation. In IF 3000 test the pressure and the temperature as they were measured upstream the release were 19 bars and 37 K, respectively. These conditions are referred to as the reservoir conditions. The mass flow rate was measured to be equal to 0.00455 kg/s. In IF 3004 test the reservoir pressure was 29 bars, the reservoir temperature was 36 K and the measured mass flow rate was 0.00802 kg/s.

According to the measured reservoir pressure and temperature conditions in both tests (IF 3000 and IF 3004) the hydrogen is in supercritical single phase state with high liquid-like densities (approximately 26 and 49 kg/m^3, respectively calculated with the real gas equation of state available in NIST [9]).

To measure the axial hydrogen concentration gas-sample taking cylinders were placed along the jet centerline at several diameter distances. At some distance from the source it was observed that hydrogen concentration was inclined from the jet trajectory due to buoyancy, especially for small mass flow rates. Those data points were omitted, in order to exclude this effect and indentify the undisturbed axial concentration decay in cryogenic jets. Therefore, there are available experimental data up to 3 and 4 m downwind the nozzle for IF 3000 and IF 3004, respectively.

3.0 SIMULATION SET UP

3.1 Governing equations

For the simulation performed the ADREA-HF CFD code was used, which solves the conservation equations for the mixture and the conservation equation for the mass fraction of hydrogen. The set of equations are:

$$\frac{\partial \rho}{\partial t} + \frac{\partial \rho u_i}{\partial x_i} = 0 \tag{1}$$

$$\frac{\partial \rho u_i}{\partial t} + \frac{\partial \rho u_j u_i}{\partial x_j} = -\frac{\partial P}{\partial x_i} + \rho g_i + \frac{\partial}{\partial x_j}\left((\mu + \mu_t)\left(\frac{\partial u_i}{\partial x_j} + \frac{\partial u_j}{\partial x_i}\right)\right) \quad (2)$$

$$\frac{\partial \rho H}{\partial t} + \frac{\partial \rho u_j H}{\partial x_j} = \frac{\partial}{\partial x_j}\left(\frac{\mu_{eff}}{\mathrm{Pr}_t}\frac{\partial H}{\partial x_j}\right) + \frac{dP}{dt} \quad (3)$$

$$\frac{\partial \rho q_i}{\partial t} + \frac{\partial \rho u_j q_i}{\partial x_j} = \frac{\partial}{\partial x_j}\left(\left(\rho D + \frac{\mu_t}{Sc_t}\right)\frac{\partial q_i}{\partial x_j}\right) \quad (4)$$

In the above equations ρ is the mixture density (kg/m^3), u is the velocity vector (m/s), P is the pressure (Pa), g is the gravitational acceleration vector (m/s^2), μ, μ_t, μ_{eff} are the laminar, turbulent and effective viscosity respectively (kg/m/s), Pr_t is the dimensionless turbulent Prandtl number, D is the molecular diffusivity of hydrogen to air (m^2/s), λ is the thermal conductivity (W/K/m), Sc_t is the dimensionless turbulent Schmidt number, H is the enthalpy, and q is the mass fraction. Prandtl number and Schmidt number are both set equal to 0.72. The subscripts i, j denotes the component i and the Cartesian j coordinate, respectively.

The mixture density is calculated based on the density and mass fraction of each component in the mixture:

$$\frac{1}{\rho} = \sum \frac{q_i}{\rho_i} \quad (5)$$

For the sum of all components' mass fraction the following relationship is applied:

$$\sum q_i = 1 \quad (6)$$

The reservoir conditions correspond to low temperatures and high pressures. Under such conditions the hydrogen deviates from the ideal gas behavior. Therefore, during the simulations the Peng-Robinson equation of state (EOS) for real gases is used for the hydrogen. In Figure 1 the compressibility factor (z) of hydrogen with respect to the pressure at constant temperature equal to the reservoir temperature of each simulated test (IF 3000 and IF 3004) is shown.

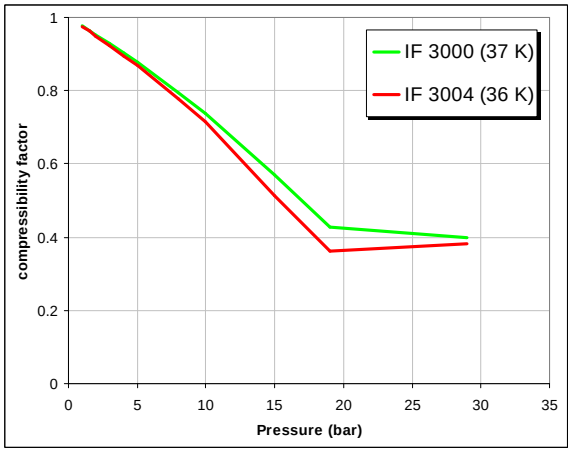

Figure 1. The compressibility factor of hydrogen versus pressure at the reservoir temperatures of tests IF 3000 and IF 3004, as calculated using the Peng-Robinson EOS.

The compressibility factor was calculated by the ratio of the density derived by the ideal EOS to the density derived by Peng-Robinson EOS. Figure 1 shows that at the reservoir pressures of the simulated experiments (19 and 29 bars) the compressibility factor is way below unity; therefore, the ideal gas assumption at nozzle conditions could lead to false results.

The reservoir density of hydrogen, that was derived using the Peng-Robinson EOS is 29.13 and 51.22 kg/m^3 for the IF 3000 and IF 3004, respectively, which are not very different from the values that are calculated using the NIST real gas equation of state for normal hydrogen, as in [1].

3.2 Numerical details

For the time integration of the conservation equations the 1st order fully implicit scheme was used, while for the convective terms the QUICK (3rd order) numerical scheme was used. A constant CFL number equal to 10 was imposed, in order to restrict the increase of time step.

The west (behind the nozzle) and bottom domains were wall boundaries and no-slip condition was imposed. The other boundaries were set as open boundaries. The constant pressure boundary condition for the normal velocity is applied and zero gradient was imposed for the rest variables, except for temperature and hydrogen mass fraction, for which either a zero gradient boundary condition was applied if outflow occurs or a given value boundary condition (equal to the initial value) if inflow occurs.

3.3 Source modeling

The main challenge for the simulation was to calculate the conditions (pressure and temperature) at the nozzle. With the help of the conservation of mechanical energy and assuming that the process is reversible and adiabatic (isentropic process) the mass flux at the nozzle can be derived by [10],

$$\dot{m}'' = \rho_n u_n = \rho_n \left[2 \int_{\rho_n}^{\rho_0} \frac{1}{\rho} dP \right]^{\frac{1}{2}} \tag{7}$$

where $\dot{m}''$ - mass flux, kg/m^2/s; ρ - density, kg/m^3; u - velocity, m/s; P - pressure, Pa. The index n and 0 are for nozzle and reservoir conditions respectively. The real gas properties should be taken under consideration in the above equation. If two-phase conditions prevail at nozzle, then the mixture density is calculated with the help of the vapor quality (vapor mass fraction). The task is to find the maximum mass flux, which corresponds to the chocked flow. That is to find the pressure P_n such that the $\dot{m}''$ is the maximum. A previous study [10] regarding this methodology showed very good agreement between the calculated and the measured flow rate based on NASA cryogenic critical flow data [11,12].

The sonic velocity at the nozzle as estimated using the above methodology [13] is equal to 451 and 718 m/s in IF 3000 and IF 3004, respectively. The mass flow rate at the nozzle is known and equals the measured mass flow rate upstream of the nozzle, neglecting any pressure losses along the pipe. Therefore, using the following equation the density of the real hydrogen at the nozzle can be derived,

$$\dot{m} = \rho_n u_n A_n \tag{8}$$

where $\dot{m}$ - mass flow rate, kg/s; A - area, m^2. The discharge coefficient of the nozzle is assumed equal to 1.

The calculated density corresponds to a pair of pressure and temperature. To estimate the conditions at the nozzle a pair of pressure and temperature below the reservoir pressure and temperature following

an isentropic path was sought that provides the calculated density. The entropy-temperature diagram [14] for hydrogen was used for this process. It was found that in both experiments two-phase flow occurs at the nozzle. For IF 3000 the temperature at the nozzle was estimated to be, approximately, 30.5 K and the pressure was the saturated pressure at this temperature, i.e 8.7 bars. For the IF 3004 the temperature at the nozzle was estimated to be, approximately, 28 K and the pressure was the saturated pressure at this temperature (5.7 bars).

In high-pressure releases an under-expanded jet is formed close to the release point, which will rapidly expands to atmospheric pressure through a series of shock. Several approaches have been proposed to model the source of high pressure under-expanded jet, in order to avoid the computationally expensive grid resolution near the source. These approaches introduce the notional nozzle (see Figure 2), where the jet is expanded to atmospheric pressure. Applying mass balance through the expansion area, the diameter (pseudo-diameter) at the notional nozzle is calculated. The velocity at the nozzle is considered sonic and the velocity at the notional nozzle can be either assumed sonic or calculated by the momentum balance.

In this work, in order to estimate the conditions in the under-expanded jet two different approaches were employed: the Ewan and Moodie approach and a modification to that approach (modified Ewan and Moodie approach) that is introduced here. Ewan and Moodie [7] used the mass conservation equation from the nozzle to the notional area (level 3, see Figure 2) similar to Birch 84 [15], in order to calculate the expanded area. The velocity at the notional location is considered sonic, at atmospheric pressure and with the same mass flow rate as at the nozzle (level 2). Ewan and Moodie also suggested that the temperature at level 3 is the same as at level 2, based on experimental data of under-expanded air jets at pressure up to 20 bars. The equations to calculate the velocity at level 3 and the pseudo-source area are:

$$u_3 = \sqrt{R_g \gamma T_3} \tag{9}$$

$$A_{ps} = \frac{\dot{m}}{\rho_3 u_3} \tag{10}$$

where R_g - the specific gas constant, J/kg/K; γ - the adiabatic index; T - the temperature, K. For the adiabatic index of hydrogen the value 1.4 was used.

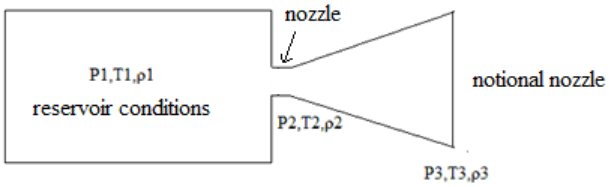

Figure 2. Under-expanded jet from the reservoir (level 1) though the nozzle (level 2). The gas is expanded to a notional location (level 3).

In the modified Ewan and Moodie approach it is no longer assumed that the velocity at level 3 is sonic. Instead in order to calculate the velocity at level 3 the momentum conservation equation through the expansion area is employed, similar to Birch 87 [8]. The assumptions that the pressure at level 3 is reduced to ambient and that the temperature at level 3 is the same as at level 2 are retained. Therefore, equation (10) calculates the pseudo-source area, and the velocity at level 3 is derived by:

$$u_3 = u_2 + \frac{A_2}{\dot{m}}(P_2 - P_3) \tag{11}$$

Using both approaches, single phase release occurs at the notional nozzle. Only gaseous hydrogen exists, because the pressure is the ambient pressure and the estimated temperature is above the saturation temperature of hydrogen at this pressure.

3.4 Computational Grid

The computational domain is 4.012 x 0.5 x 2 m and 4.512 x 0.5 x 2 m for IF 3000 and IF 3004, respectively. In the x-direction the domain was extended 12 mm upwind the nozzle, while in the z-direction the domain was extended equally above the source and below it. Symmetry along the y-axis was assumed. The centre of the source is placed at coordinates (0,0,1) in the domain. For the source modelling a square solid area was considered with area equal to the pseudo-source area as calculated using the approaches that are described in the previous paragraph. This solid area was set as inlet boundary with boundary conditions the hydrogen inlet conditions. A parallelepiped box was placed behind the source, in order to model the pipe. The cells along the pipe were fully blocked. One cell covered the symmetric (half) source area and expansion ratios equal to 1.05-1.12 were used (refinement was imposed near the source). Small expansion ratios were set in an area close to the source along x-and z-direction (1.05 and 1.09 respectively). In the x-direction, 0.1 m downwind the source and up to the end of the domain an expansion ratio equal to 1.08 was applied. In the y-direction the expansion ratio was constant equal to 1.12. Dependent on the experiment and the approach employed to calculate the pseudo-source area the grid size varied, because the pseudo-source area was different. In the simulation of the IF 3000 test the grid consisted of 167 552 and 195 534 cells using the Ewan and Moodie and the modified Ewan and Moodie approach, respectively. In the simulation of the IF 3004 test the grid consisted of 136 320 and 182 952 cells using the Ewan and Moodie and the modified Ewan and Moodie approach, respectively. Figure 3 shows the grid on the symmetry plane and on the nozzle along the x-plane that was used in the simulation of the IF 3000 test.

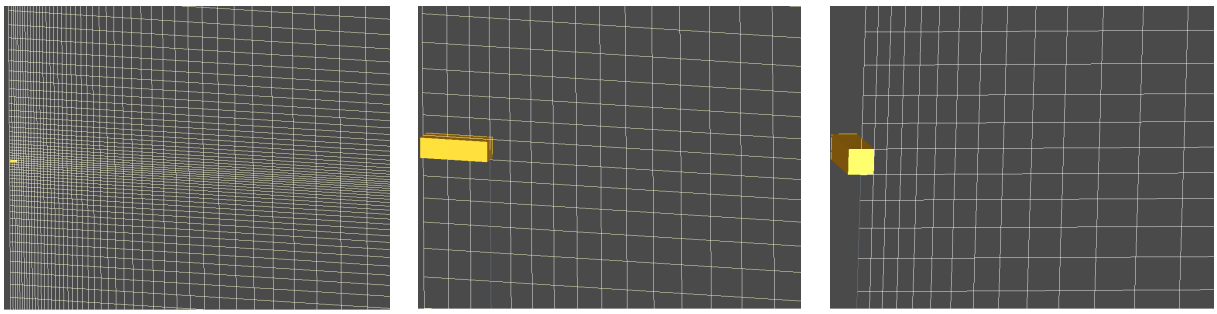

Figure 3. The grid that was used in the IF 3000 simulation using the Ewan and Moodie approach on the symmetry plane (left), in a zoomed area close to the release on the symmetry plane (centre) and on the nozzle along the x-plane (right).

Two finer grids were tested for both experiments. The Ewan and Moodie approach was applied for the grid sensitivity study. In the first finer grid two cells were applied along the symmetric (half) source area of each experiment, while all other grid characteristics (expansion ratio, refinement points etc.) were the same as in the coarse grid case. It consisted of 243 648 and 196 080 cells in IF 3000 and IF 3004, respectively. In the second finer grid one cell covered the source area, but smaller expansion ratios than in the coarse grid, varying from 1.04-1.09 were applied in all directions. The total number of cells was 349 596 and 255 255 in the IF 3000 and IF 3004, respectively. The computational results showed no discrepancies (see Section 4.0), therefore, the coarse grid can be considered that provides grid independent results.

In general, for the simulation setup the “best practices guidelines for CFD model evaluation” that have been developed within the SUSANA project [6] have been applied. A grid sensitivity study was performed. The boundary conditions were set as proposed in the Model Protocol Evaluation (MEP), and the source of the high-pressure release was modeled based on notional nozzle approach. Finally, high order numerical scheme were applied, in order to reduce the numerical diffusion.

4.0 RESULTS

Figure 4 displays the comparison between the three different grids that were tested for each experiment. It is shown that the coarse grid used in this study leads to grid independent results. The finer grid with one cell on the symmetric source area and the finer grid with two cells on the symmetric source do not exhibit any significant discrepancy from the coarse grid. Therefore, the coarse grid is used for the rest of the analysis.

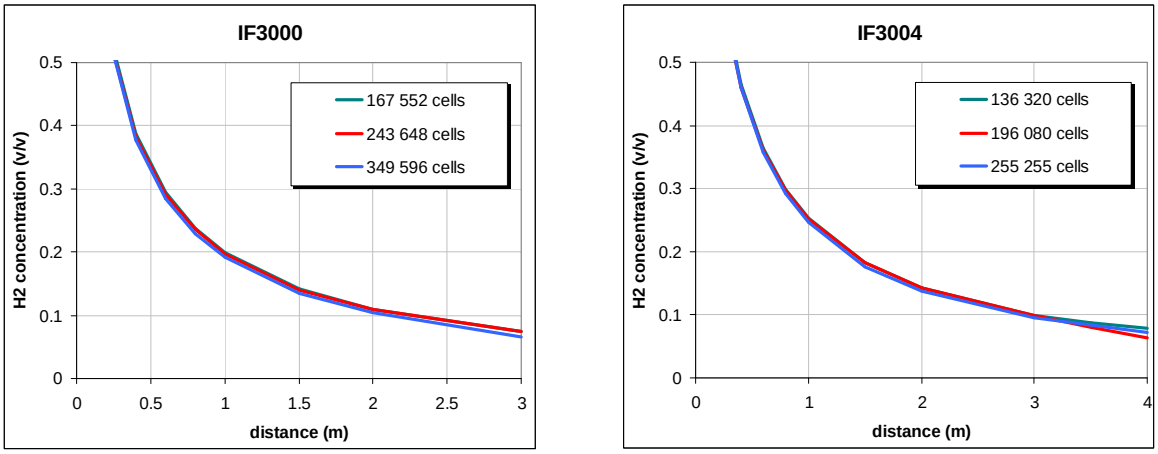

Figure 4. Comparison of the three different grids used to perform the grid sensitivity study for the IF 3000 experiment (left) and the IF 3004 experiment (right).

Figure 5 and Figure 6 show the hydrogen concentration by volume (v/v) along the jet centerline and at steady state in comparison with the measurements for IF 3000 and IF 3004 experiment, respectively. The predictions with both the Ewan and Moodie approach and the modified Ewan and Moodie approach are presented.

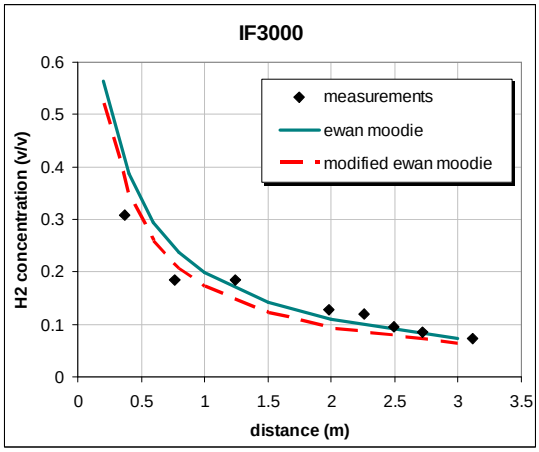

Figure 5. The predicted and measured hydrogen concentration by volume (v/v) along the jet centreline for the IF 3000 experiment.

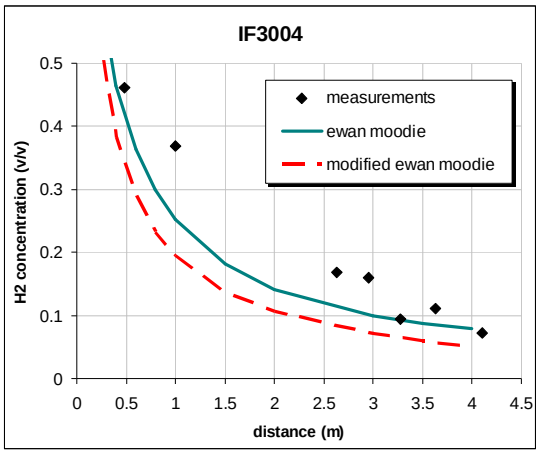

Figure 6. The predicted and measured hydrogen concentration by volume (v/v) along the jet centreline for the IF 3004 experiment.

The predictions of the IF 3000 experiment tend to over-predict the concentration close to the nozzle using both approaches, while they are in good agreement for the sensors after 1 m downwind the release. The relative error at the closest to the nozzle sensor is approximately 30% and 16% for the Ewan and Moodie and the modified Ewan and Moodie approach, respectively. In general, the Ewan and Moodie approach is in better agreement with the measurements at all distances except for the distances very close to the nozzle, where the modified Ewan and Moodie performs better.

In the IF 3004 both approaches under-predict the concentration at most distances downwind the release. The Ewan and Moodie approach performs better than the modified Ewan and Moodie, which underestimates more the hydrogen concentration at all distances. The relative error of the results using the Ewan and Moodie approach is about 16% at the closest to the nozzle sensor, whilst at the further distances (last three sensors) is varied from 3-24%.

In general, both approaches are consistent with the measurements, however, the Ewan and Moodie approach seems to perform better in both experiments.

5.0 CONCLUSIONS

CFD simulations of cryogenic hydrogen release based on the cryogenic hydrogen jet experiments carried out by KIT have been performed in this work within the SUSANA project. Two experiments were chosen for simulation the IF 3000 and the IF 3004. These experiments are related to hydrogen release though a 1 mm nozzle at temperature 37 and 36 K and pressure 19 and 29 bars, respectively. The mass flow rate was measured during the experiments using a mass flow meter and it was 0.0045 and 0.00802 kg/sec for the IF 3000 and IF 3004, respectively. The simulation setup was based on the Model Protocol Evaluation (MEP) for safety analysis of hydrogen and fuel cell technologies that is developing within the SUSANA project.

Two different approaches have been used to model the under-expanded jet: the Ewan and Moodie approach and a modification of the Ewan and Moodie approach that has been considered in the present work. In both approaches the mass balance between nozzle conditions and the conditions at the notional nozzle was applied. The difference between the two approaches was that in the Ewan and Moodie approach sonic velocity is considered at the notional area, while in the modified Ewan and Moodie approach the momentum balance through the expansion area was used, in order to derive the velocity at the notional nozzle. In both approaches the temperature at the notional nozzle is the same as the temperature at the actual nozzle and the pressure is the ambient pressure.

The main challenge was to estimate the nozzle conditions (temperature and pressure). To calculate the nozzle conditions isentropic process was assumed. Several pairs of temperatures and pressures along an isentropic path, using the T-S diagram, were considered until the density at the nozzle was obtained. The density corresponding to the nozzle temperature-pressure conditions was derived by the measured mass flow rate, the nozzle area and the velocity at the nozzle [13]. In both simulated experiments two-phase flow was found at the nozzle. However, at the notional nozzle only vapor phase flow occurred.

The predictions were consistent with the measurements for both experiments and using both under-expanded jet modeling approaches. However, the Ewan and Moodie approach exhibited better performance than the modified Ewan and Moodie approach in both experiments. Comparing the performance of the simulations of the two experiments, the least satisfactory agreement was found in the computational results of the IF 3004 experiment, which had the higher mass flow rate. The prediction underestimated the hydrogen concentration almost at all distances in the IF 3004.

In the future, simulations of more tests related to cryogenic hydrogen jet experiments will give better insight on the performance of the CFD simulations for cryogenic releases. Finally, the effect of the condensation of ambient humidity on hydrogen dispersion could also be investigated.

6.0 ACKNOWLEDGEMENTS

The authors would like to thank the Fuel Cell and Hydrogen Joint Undertaking for the co-funding of the SUSANA project (Grant-Agreement FCH-JU-325386). The authors would also like to thank Mikhail Kuznetsov for the useful discussion and the information that were provided regarding the experiments.

7.0 REFERENCES

1. Friedrich, A., Breitung, W., Stern, G. , Veser, A., Kuznetsov, M., Fast, G., Oechsler, B., Kotchourko, N., Jordan, T., Travis, J. R., Xiao, J., Schwall, M. and Rottenecker, M., Ignition and heat radiation of cryogenic hydrogen jets, *Int. J. Hydrogen Energy*, **37**, No. 22, 2012, pp. 17589–17598.
1. Gallego, E., Migoya, E., Martín-Valdepeñas, J.M., Crespo, A., García, J., Venetsanos, A., Papanikolaou, E., Kumar, S., Studer, E., Dagba, Y., Jordan , T. , Jahn, W., HZiset, S., Makarov, D., Piechna, J., An intercomparison exercise on the capabilities of CFD models to predict distribution and mixing of H2 in a closed vessel, *Int. J Hydrogen Energy*, **32**, 2007, pp. 2235-2245.
2. Papanikolaou, E.A., Venetsanos, A. G., Heitsch, M., Baraldi, D., Huser, A., Pujol, J., Garcia, J. and Markatos, N., HySafe SBEP-V20: Numerical studies of release experiments inside a naturally ventilated residential garage, *Int. J. Hydrogen Energy*, **35**, No. 10, 2010, pp. 4747–4757.
3. Venetsanos, A.G., Papanikolaou, E. and Bartzis, J. G., The ADREA-HF CFD code for consequence assessment of hydrogen applications, *Int. J. Hydrogen Energy*, **35**, No. 8, 2010, pp. 3908–3918.
4. “SUSANA project webpage”, http://www.support-cfd.eu/.
5. Venetsanos, A.G, Tolias, I.C., Giannissi, S.G., Coldrick, S., Ren, K., Kotchourko, A., Makarov, D., Chernyavsky, B., Molkov, V., D3.1 Guide to best practices in numerical simulations, Rep. SUSANA Project.
6. Ewan, B. C. R. and Moodie, K., Structure and Velocity Measurements in Underexpanded Jets,” *Combust. Sci. Technol.*, **45**, No. 5–6, 1986, pp. 275–288.
7. Birch, A. D., Hughes, D. J. and Swaffield, F., Velocity decay of high pressure jets, *Combust. Sci. Technol.*, **45**, 1987, pp. 161–171.
8. “NIST”, http://webbook.nist.gov/.

9. Travis, J., Koch, D. and Breitung, W., A homogeneous non-equilibrium two-phase critical flow model, *Int. J. Hydrogen Energy*, **37**, No. 22, 2012, pp. 17373–17379.
10. Simoneau, R. and Hendricks, R., Two-phase choked flow of cryogenic fluids in converging-diverging nozzles, NASA Tech. Rep. Pap. 1484, 1979.
11. Hendricks, R.F., Simoneau, RC, and Barrows, R.J., Two-phase choked flow of subcooled oxygen and nitrogen, NASA Tech. Rep. Pap. TN-8169, 1976.
12. "The values of the velocities were provided by KIT under private conversation."
13. Gstrein, G. and Klell, M., Stoffwerte von Wasserstoff [Properties of Hydrogen], Inst. Intern. Combust. Engines and, Thermodyn. Graz Univ. Technol., 2004.
14. Birch, A. D., Brown, D. R., Dodson, M. G. and Swaffield, F., The Structure and Concentration Decay of High Pressure Jets of Natural Gas, *Combust. Sci. Technol.*, **36**, No. 5–6, 1984, pp. 249–261.